

# Loss-of-function approach using mouse retinal explants showed pivotal roles of *Nmnat2* in early and middle stages of retinal development

Hiroshi Kuribayashi<sup>a,b,\*</sup>, Miku Katahira<sup>b</sup>, Makoto Aihara<sup>c</sup>, Yutaka Suzuki<sup>d</sup>, and Sumiko Watanabe<sup>a,b,\*</sup>

<sup>a</sup>Department of Retinal Development and Pathophysiology, and <sup>c</sup>Department of Ophthalmology, Graduate School of Medicine, and <sup>b</sup>Division of Molecular and Developmental Biology, Institute of Medical Science, The University of Tokyo, Tokyo, Japan; <sup>d</sup>Department of Medical Genome Sciences, Graduate School of Frontier Science, The University of Tokyo, Chiba, Japan

**ABSTRACT** Nicotinamide mononucleotide adenyltransferase (*Nmnat*) is a class of enzymes with three members (*Nmnat1–3*). *Nmnat1* is in nucleus and associated with Leber congenital amaurosis, a form of early-onset retinal degeneration, while *Nmnat2* is in cytoplasm and a well-characterized neuroprotective factor. The differences in their biological roles in the retina are unclear. We performed short hairpin RNA (shRNA)-based loss-of-function analysis of *Nmnat2* during mouse retinal development in retinal explant cultures prepared from early (E14.5), middle (E17.5), or late (postnatal day [P]0.5) developmental stages. *Nmnat2* has important roles in the survival of retinal cells in the early and middle stages of retinal development. Retinal cell death caused by *Nmnat2* knockdown could be partially rescued by supplementation with NAD or nicotinamide mononucleotide (NMN). Survival of retinal cells in the late stage of retinal development was unaffected by *Nmnat2*, but differentiation of Müller glia was controlled by *Nmnat2*. RNA-Seq analyses showed perturbation of gene expression patterns by shRNAs specific for *Nmnat1* or *Nmnat2*, but gene ontology analysis did not provide a rational explanation for the phenotype. This study showed that *Nmnat2* has multiple developmental stage-dependent roles during mouse retinal development, which were clearly different from those of *Nmnat1*, suggesting specific roles for *Nmnat1* and *Nmnat2*.

## Monitoring Editor

Rachel Brewster  
University of Maryland,  
Baltimore County

Received: Mar 7, 2022

Revised: Oct 20, 2022

Accepted: Oct 28, 2022

This article was published online ahead of print in MBoC in Press (<http://www.molbiolcell.org/cgi/doi/10.1091/mbc.E22-03-0078>) on November 2, 2022.

\*Address correspondence to: Hiroshi Kuribayashi (krbyshrs5926@gmail.com); Sumiko Watanabe (sumiko@g.ecc.u-tokyo.ac.jp).

Abbreviations used: act-Casp3, active caspase-3; DAVID, database for annotations, visualization and integrated discovery; DEGs, differentially expressed genes; EGFP, enhanced green fluorescent protein; GO, gene ontology; GSEA, gene set enrichment analysis; GS, glutamine synthetase; INL, inner nuclear layer; LCA, leber congenital amaurosis; NMN, mononucleotide; NAD, nicotinamide adenine dinucleotide; NMN, nicotinamide mononucleotide; *Nmnat*, nicotinamide mononucleotide adenyltransferase; NaAD, nicotinic acid adenine dinucleotide; NaMN, nicotinic acid mononucleotide; ONL, outer nuclear layer; Parps, poly (ADP-ribose) polymerases; PARYlation, poly(ADP-ribosyl)ation; qPCR, quantitative polymerase chain reaction; RGCs, retinal ganglion cells; RPE, retinal pigment epithelium; RPC, retinal progenitor cell; shRNA, short hairpin RNA; Sirts, sirtuins; Sarm1, sterile alpha and TIR motif containing 1; TPM, transcripts per million; UMAP, uniform manifold approximation and projection.

© 2023 Kuribayashi et al. This article is distributed by The American Society for Cell Biology under license from the author(s). Two months after publication it is available to the public under an Attribution-Noncommercial-Share Alike 4.0 International Creative Commons License (<http://creativecommons.org/licenses/by-nc-sa/4.0>).

"ASCB®," "The American Society for Cell Biology®," and "Molecular Biology of the Cell®" are registered trademarks of The American Society for Cell Biology.

## INTRODUCTION

Nicotinamide adenine dinucleotide (NAD) is an essential molecule for major energy production pathways, including glycolysis, the tricarboxylic acid cycle, and fatty acid oxidation. NAD is a critical cosubstrate for the NAD-dependent enzymes Sirtuins (Sirts) and poly (ADP-ribose) polymerases (Parps) and plays roles in multiple cell signaling pathways contributing to development, homeostasis, and aging (Imai and Guarente, 2016; Covarrubias et al., 2021). Nicotinamide mononucleotide adenyltransferases (*Nmnats*) are essential enzymes in NAD synthesis pathways and catalyze the conversion of mononucleotide (NMN) to NAD or of nicotinic acid mononucleotide (NaMN) to nicotinic acid adenine dinucleotide (NaAD). There are three isoforms of *Nmnat*, *Nmnat1*, *Nmnat2*, and *Nmnat3*, which were reported to have different subcellular localizations in the nucleus, cytoplasm, and mitochondria, respectively (Berger et al., 2005).

Mutation of *Nmnat1*, the nuclear NAD synthase, has been shown to cause Leber congenital amaurosis (LCA), which is an early-onset retinal photoreceptor degeneration disease (den Hollander et al., 2008), and several groups have attempted to elucidate the

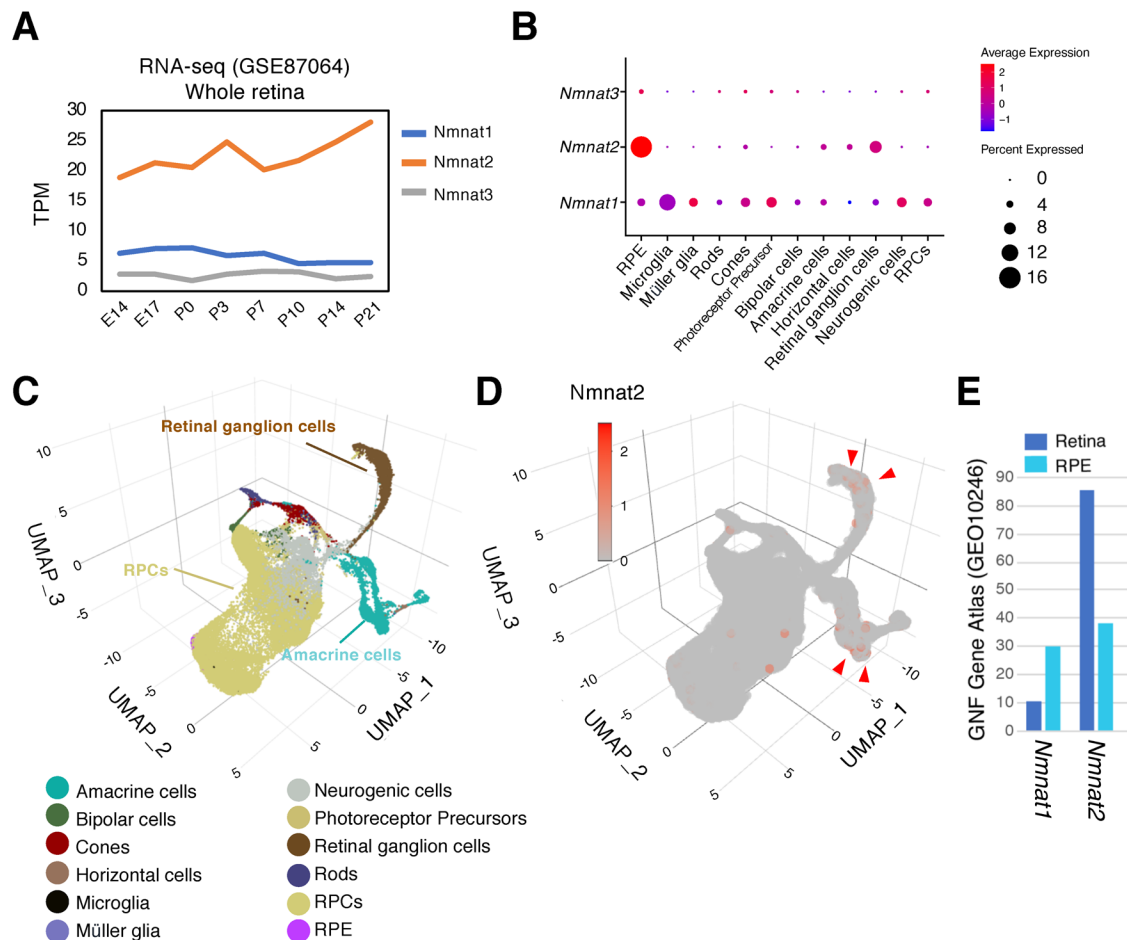


**FIGURE 1:** Gene expression patterns of *Nmnat1*, *Nmnat2*, and *Nmnat3* during retinal development. (A) Transition of mRNA expression of *Nmnat* family genes during mouse retinal development was examined using publicized RNA-Seq data (GSE87064). The expression levels for *Nmnat* family genes *Nmnat1*, *Nmnat2*, and *Nmnat3* were quantified as transcripts per million (TPM). (B) Dotplot showing spatial expression patterns of *Nmnat* family genes (Y axis) across retinal cell subtypes (X axis). Dot color indicates average expression level and dot diameter indicates proportion of cells expressing each gene in each retinal cell subtype. RPE, retinal pigment epithelium; RPCs, retinal progenitor cells. (C, D) UMAP-dimension reduction of single cell RNA-Seq of developing mouse retina (GSE113684). Cells were colored by annotated retinal cell types as determined by marker gene expression, (C) or the expression level of *Nmnat2*, (D). Red arrowheads in D indicate cells expressing *Nmnat2* with relatively high level. (E) Expression of *Nmnat1* and *Nmnat2* in retina and RPE examined by the microarray (GEO1-246).

underlying mechanisms (Falk *et al.*, 2012; Koenekoop *et al.*, 2012). *Nmnat1V9M/V9M* mice harbor a p.Val9Met mutation in *Nmnat1* and show a retinal degeneration-like phenotype at 3 wk old, similar to the retina of infants with LCA (Greenwald *et al.*, 2016). Furthermore, we have shown that short hairpin RNA (shRNA)-mediated suppression of *Nmnat1* led to retinal progenitor cell (RPC) death in mouse retina explant culture (Kuribayashi *et al.*, 2018).

*Nmnat2* has attracted attention as a neuroprotective factor (Zhai *et al.*, 2008; Ali *et al.*, 2013; Ruan *et al.*, 2015). Wallerian degeneration, which is a process of active neural degeneration of distal axon stumps following physiological injury, is a well-studied example of the involvement of *Nmnat2* in neuronal degeneration (Mack *et al.*, 2001; Gilley and Coleman, 2010; Conforti *et al.*, 2014). This process is known to be activated by loss of *Nmnat2* and delayed by overexpression of *Nmnat2* (Feng *et al.*, 2010; Gilley and Coleman, 2010). Mice lacking *Nmnat2* show severe peripheral axon defects and innervation defects of major organs and muscles, leading to death in the perinatal stage (Hicks *et al.*, 2012). Sterile alpha and TIR motif-containing 1 (*Sarm1*) has emerged as a novel neuroprotective factor

with NADase activity (Gilley *et al.*, 2015; Essuman *et al.*, 2017). Furthermore, although *Nmnat2* knockout is lethal, mice lacking both *Nmnat2* and *Sarm1* are viable (Gilley *et al.*, 2015). These results suggest that *Nmnat2* is essential for survival of neurons, probably through maintenance of appropriate levels of NAD, but the roles of *Nmnat2* in retinal development and maintenance remain to be elucidated.

We performed shRNA-based loss-of-function analysis of *Nmnat2* using mouse retinal explants harvested from multiple developmental stages, revealing that *Nmnat2* contributes to retinal cell survival and differentiation in a developmental stage-specific manner.

## RESULTS

### *Nmnat2* is uniquely expressed in retinal subtypes during retinal development

We showed previously that the level of *Nmnat2* expression was relatively stable in the retina from fetal to adult mouse stage (Kuribayashi *et al.*, 2018). Public RNA-Seq data (GSE87064) and our previous RNA-Seq results (GSE71462; unpublished data) for developing

mouse retinas showed that the expression level of *Nmnat2* was highest among *Nmnat* family genes in the whole retina during mouse retinal development (Figure 1A). The major population of retinal subtypes of embryonic retinas is RPC, suggesting high and constant expression levels of *Nmnat2* in RPC. We previously performed RNA-Seq analysis of retinal CD73-positive (CD73+) rod photoreceptor and CD73-negative (CD73-) other cells and showed that *Nmnat2* is expressed in CD73- cells, but only negligible values were observed with CD73+ cells (Kuribayashi *et al.*, 2018). A public scRNA-Seq dataset (GSE118614) for the developing mouse retina also showed low expression of *Nmna2* in rod photoreceptors (Figure 1, B–D); these data consistently suggested that *Nmnat1* and very low *Nmnat2* are expressed in rod photoreceptor lineage. In the scRNA-Seq results, the expression of *Nmnat1* was low but was detected in a variety of retinal cell types, including RPCs, neurogenic cells, photoreceptor precursors, cone photoreceptors, and Müller glia (Figure 1B), while *Nmnat2* was nearly predominantly expressed in retinal ganglion cells (RGCs), amacrine cells, and horizontal cells (Figure 1, B–D). In the scRNA-Seq data, RPCs showed only negligible expression of *Nmnat2*, which is in contrast to the data of Figure 1A, and we do not have a rational explanation for this inconsistency. Interestingly, retinal pigment epithelium (RPE) showed the highest expression of *Nmnat2* among retinal cell types, while rod photoreceptors, bipolar cells, and RPC did not show such high level of *Nmnat2* expression (Figure 1, B–D). However, previous microarray data showed comparable or rather lower expression levels of *Nmnat2* in RPE than in retina in adult mouse (Figure 1E), suggesting that expression patterns in each subtype of retinal cells are still not conclusive.

### ***Nmnat2* is essential for RPC survival at both early and middle developmental stages**

The retinal subtypes develop in a chronologically defined order from the RPCs (Young, 1985; Cepko *et al.*, 1996; Figure 2A). Early-born retinal cell types such as RGCs, amacrine cells, horizontal cells, and cone photoreceptors are differentiated from embryonic RPCs, but late-born cell types such as bipolar cells, rod photoreceptors, and Müller glia are largely generated in postnatal stages (Figure 2A). To examine the roles of *Nmnat2* during the transition of retinal development, we performed shRNA-mediated loss-of-function analysis of *Nmnat2* using retinas isolated from mice at three different stages of development (embryonic days [E] 14.5 and 17.5 and postnatal day [P] 0.5). In all cases, cell death and cell proliferation were verified using short-term (3 d) cultured explants, and cell differentiation was evaluated using long-term (10- or 14-d) cultured explants of the retinas at E17.5 and P0.5, as shown schematically in Figure 2A.

We first confirmed that sh*Nmnat2* expression plasmids were effective in suppressing *Nmnat2* transcript expression in NIH3T3 cells (Figure 2B). To assess off-target effect of sh*Nmnat2* on other *Nmnat* family genes, we confirmed that target sequences of sh*Nmnat2* expression plasmids were not homologous to other *Nmnat* family genes, *Nmnat1* and *Nmnat3*, by BLAST search. We also examined the expression of *Nmnat1* and *Nmnat3* in NIH3T3 cells transfected with sh*Nmnat2* expression plasmids. Although we could not detect the expression of *Nmnat3* because of its low level, the expression of *Nmnat1* was not affected by sh*Nmnat2* (Figure 2C). Then we coelectroporated pU6-sh*Nmnat2* or -scramble and pCAG-EGFP into retinas isolated from E14.5 mouse embryos, and the explanted retinas were harvested on day 3. In the following section, data obtained by expression of sh*Nmnat2*-1st (target sequence is shown in *Materials and Methods*) are shown as representative data, but we obtained essentially the same results with expression of sh*Nmnat2*-2nd (target

sequence is shown in *Materials and Methods*) in the retina (unpublished data). The number of active caspase-3 (act-Casp3)-positive apoptotic cells was significantly increased in the retinas into which sh*Nmnat2* had been introduced, compared with the controls (Figure 2, D and G). On the other hand, the number of Ki67-positive proliferating cells was decreased (Figure 2, E and H). The number of BRN3B-positive RGCs was comparable between the two samples (Figure 2, F and I). However, it is notable that the efficiency of transfection into RGC lineage cells was very low, probably because RGCs start to differentiate earlier than the timing of electroporation. Therefore, it is suggested that depletion of NMNAT2 in the RGC lineage does not affect their differentiation.

We then performed electroporation as described above using retinas isolated at E17.5. The results indicated that expression of sh*Nmnat2* was associated with an increase in act-Casp3-positive cells and a decrease in Ki67-positive cells (Figure 3, A–D). Taken together, these observations suggest that *Nmnat2* is essential for survival and proliferation of RPCs in the embryonic retina.

### ***Nmnat2* plays an important role in retinal cell differentiation in the middle developmental stage**

We next examined differentiation using explants cultured for 14 d after electroporation. Due to apoptosis, the total number of EGFP-positive cells in the retinas electroporated with sh*Nmnat2* was much lower than in the controls. In addition, the subretinal distribution of EGFP-positive cells was also altered by sh*Nmnat2* expression; most of the EGFP-positive cells disappeared from the inner nuclear layer (INL), and remaining EGFP-positive cells were localized in the outer nuclear layer (ONL; Figure 3E; Supplemental Figure 1A). Immunostaining with anti-cell type specific marker antibodies showed that PNR-positive rod photoreceptors were slightly decreased in the retinas expressing sh*Nmnat2* (Figure 3, F and G). Although the numbers of glutamine synthetase (GS)-positive Müller glia were comparable, apico-basal processes of Müller glia were disrupted and the subretinal localization of Müller glia cell bodies was severely perturbed in the retinas expressing sh*Nmnat2* (Figure 3, F and G). Morphology of GFP-negative GS-positive Müller glia cells were also perturbed, suggesting noncell autonomous effects of depletion of *Nmnat2* in Müller glia. The number of CHX10-positive bipolar cells was comparable between the two samples, but ectopic bipolar cells in ONL were observed in sh*Nmnat2* expressing retinal explants (Figure 3, F and G). It is possible that the abnormal Müller glia morphology affected proper localization of bipolar cells. The numbers of Calbindin-D28k-positive horizontal cells and amacrine subsets were not changed (Figure 3, F and G), while the number of TFAP2-A-positive pan-amacrine cells was increased in the retinas expressing sh*Nmnat2* compared with the controls (Figure 3, F and G).

These results indicate that *Nmnat2* knockdown led to retinal progenitor cell death at early and middle stages of retinal development, accompanied by a decrease in rod photoreceptor cells, abnormal Müller glial morphology, perturbed bipolar cell localization, and an increase in amacrine cells.

### ***Nmnat2* had no effect on cell survival in the later developmental stage, but was required for proper cell differentiation in the retina**

We then introduced sh*Nmnat2* into the retinas isolated from mice at P0.5, as described above, which were then cultured for 3 or 10 d. Immunostaining with anti-act-Casp3 antibody showed a small but comparable number of apoptotic cells in the sh*Nmnat2*-expressing explants compared with scramble-expressing controls at 3 d in

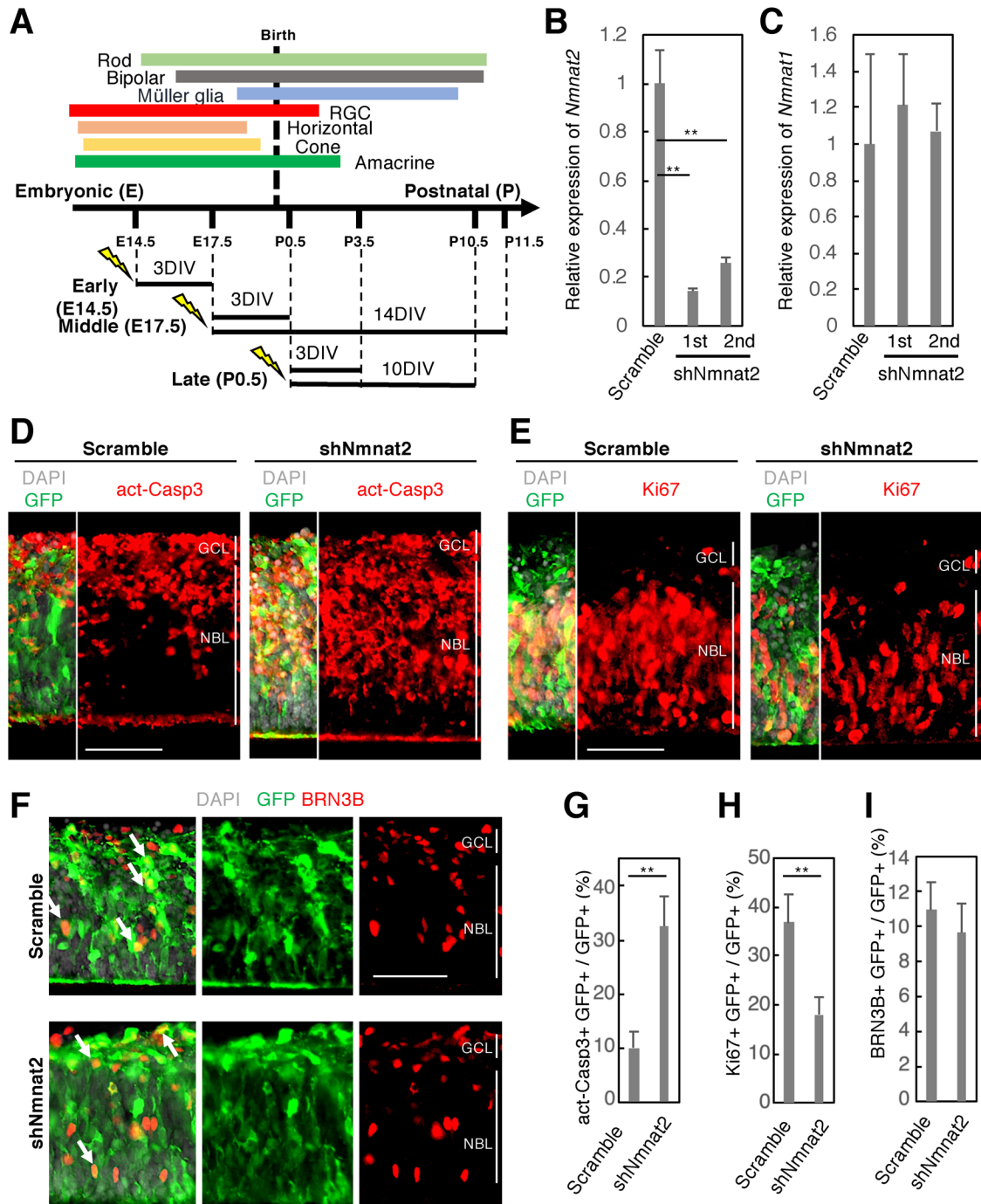


**FIGURE 2:** The roles of *Nmnat2* during early stages of mouse retinal development. (A) Schematic representation of retinal cell differentiation and experimental paradigms. Color bars indicate period of differentiation of each retinal cell type during mouse development. Plasmids encoding shNmnat2 or scramble sequences were transfected into the mouse retinas at early (E14.5), middle (E17.5), or late (P0.5) stages of mouse development, depending on the purpose of the experiment. Short-term culture of the explant retina was used to evaluate cell death and cell proliferation. Long-term culture of the retina was used to assess cell differentiation. RGC, retinal ganglion cell. (B, C) The suppressive effect of shNmnat2 on *Nmnat2* expression, B, and *Nmnat1* expression, C, was evaluated by qPCR. Scramble- or shNmnat2-expressing plasmids and EGFP-expressing plasmids were transfected together into NIH3T3 cells. After 2 d of culture, EGFP-positive cells were collected and *Nmnat2* and *Nmnat1* expression was assessed by RT-qPCR. Gene expression levels were corrected by *Gapdh* expression. (D–I) Retinas isolated from mouse embryos at E14.5 were transfected with scramble sequences or shNmnat2 encoding plasmids and EGFP expressing plasmids and harvested after 3 d of culture. Frozen sections were immunostained with anti-active-Caspase 3 (act-Casp3), D, anti-Ki67, E, or anti-BRN3B and anti-GFP, F antibody. White arrows in F indicate GFP and BRN3B double positive cells. Nuclei were visualized by staining with DAPI. Populations of active-Caspase 3+ GFP+ cells (G), Ki67+ GFP+ cells (H) and BRN3B+ GFP+ cells (I) in total EGFP+ cells are shown. NBL, neuroblastic layer; GCL, ganglion cell layer. The means and standard deviations were calculated using three independent samples. Scale bar = 50  $\mu$ m.

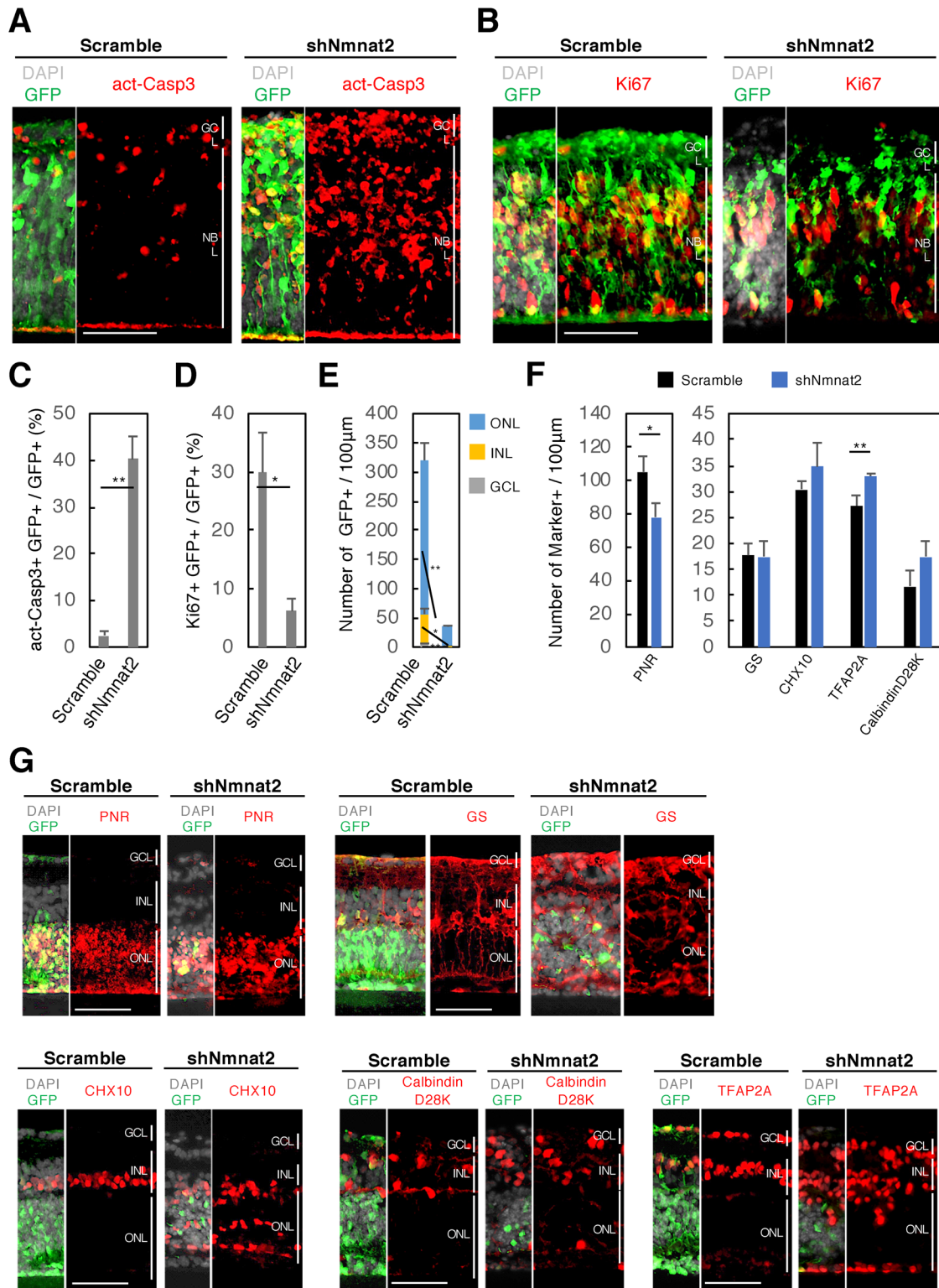


**FIGURE 3:** The roles of Nmnat2 during middle stages of mouse retinal development. Retinas isolated from mouse embryos at E17.5 were transfected with scramble sequences- or shNmnat2-encoding plasmids and EGFP expressing plasmids and harvested after 3, A–D, or 14, E–G, days of culture. (A–D) Frozen sections were immunostained with anti-act-Casp3, A, and anti-Ki67, B, antibody. Nuclei were visualized by staining with DAPI. Population (%) of active-Caspase 3+ GFP+ cells, C, and Ki67+ GFP+ cells, D, in total EGFP+ cells are shown. (E) Frozen sections were immunostained with anti-GFP antibody, and subretinal distribution of EGFP+ cells is counted. The values are means of three independent samples with standard deviations. ONL, outer nuclear layer; INL, inner nuclear layer; GCL, ganglion cell layer. (F, G) Retinal subtypes were costained with anti-EGFP- and anti-cell type specific marker antibodies, G. The numbers of each cell specific marker+ cells per 100 µm section was compared between scramble-expressing retinas and shNmnat2-expressing retinas, F. The means and standard deviations were calculated using three independent samples. Scale bar = 50 µm.

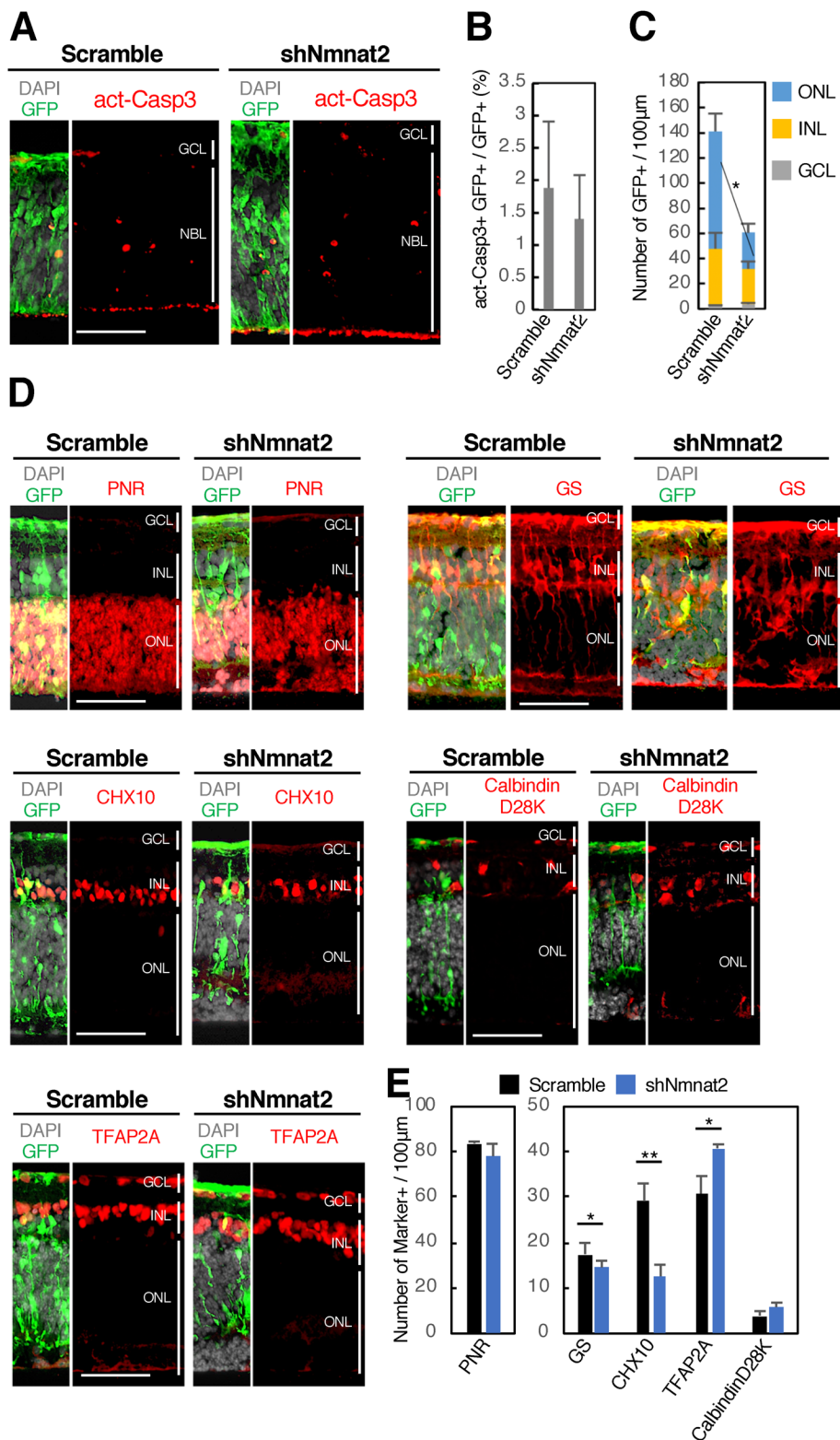


**FIGURE 4:** The roles of Nmnat2 during late stages of mouse retinal development. Mouse retinas at P0.5 were transfected with scramble sequences or shNmnat2-encoding plasmids and EGFP-expressing plasmids and harvested after 3, A, B, or 10, C–E, days of culture. (A) Frozen sections were immunostained with anti-active-Caspase 3 antibody and anti-EGFP antibody. (B) Proportions of active-Caspase 3+ EGFP+ cells in total EGFP+ cells. (C) Frozen sections were immunostained with anti-EGFP antibody, and subretinal distributions of EGFP+ cells were compared. ONL, outer nuclear layer; INL, inner nuclear layer; GCL, ganglion cell layer. (D, E) Retinal subtypes were costained with anti-EGFP and anti-cell specific marker antibodies, D. The number of cell specific marker+ cells per 100-μm section was calculated, E. In B, C, and E,

culture (Figure 4, A and B). However, with longer culture (10 d), the total number of EGFP-positive cells was decreased in the shNmnat2-expressing retinas, especially in the ONL (Figure 4C; Supplemental Figure 1B). Furthermore, most of the EGFP-positive cells in the INL of shNmnat2-expressing retinas had apico-basal processes (Figure 4D). We found a comparable number of PNR-positive rod photoreceptors between shNmnat2-expressing samples and scramble-expressing controls (Figure 4, D and E). However, the numbers of GS-positive Müller glia and CHX10-positive bipolar cells were slightly decreased and the number of TFAP2A-positive amacrine cells was increased in the shNmnat2-expressing explants (Figure 4, D and E).

By stepwise loss-of-function analyses of Nmnat2 from early to late retinal development, we found differential roles of Nmnat2 during transition of retinal development.

#### Nmnat2 suppression did not affect whole-cell NAD level and posttranslational modification

We examined whether suppression of Nmnat2 expression affected cellular NAD level. The plasmids were transfected into the retinas at E17.5, and whole-cell NAD level was measured after 3 d in culture. We did not observe significant differences in NAD levels between shNmnat2-expressing and control explants (Supplemental Figure 2).

Sirts and Parps are enzymes that require NAD for their activities (Finnin *et al.*, 2001; Kim *et al.*, 2004). As Sirts and Parps are acetyltransferases and poly(ADP-ribose) polymerases, respectively, lysine acetylation, histone acetylation, and poly(ADP-ribosyl)ation (PARylation) levels were examined. Retinal cells at E17.5 were transfected, and explants cultured for 2 d were examined by Western blotting. We found that no obvious changes in PARylation, lysine acetylation, or histone H3 and histone H4 acetylation levels between shNmnat2 and scramble groups (Supplemental Figure 3, A–E).

#### Administration of NAD rescued apoptosis in the retina transfected with shNmnat2 expression plasmid

Although perturbation of NAD level by shNmnat2 was not detected, we suspected that modulation of the subcellular localization of NAD by shNmnat2 may

the means and standard deviations were calculated using three independent samples. Scale bar = 50 μm in A and D.

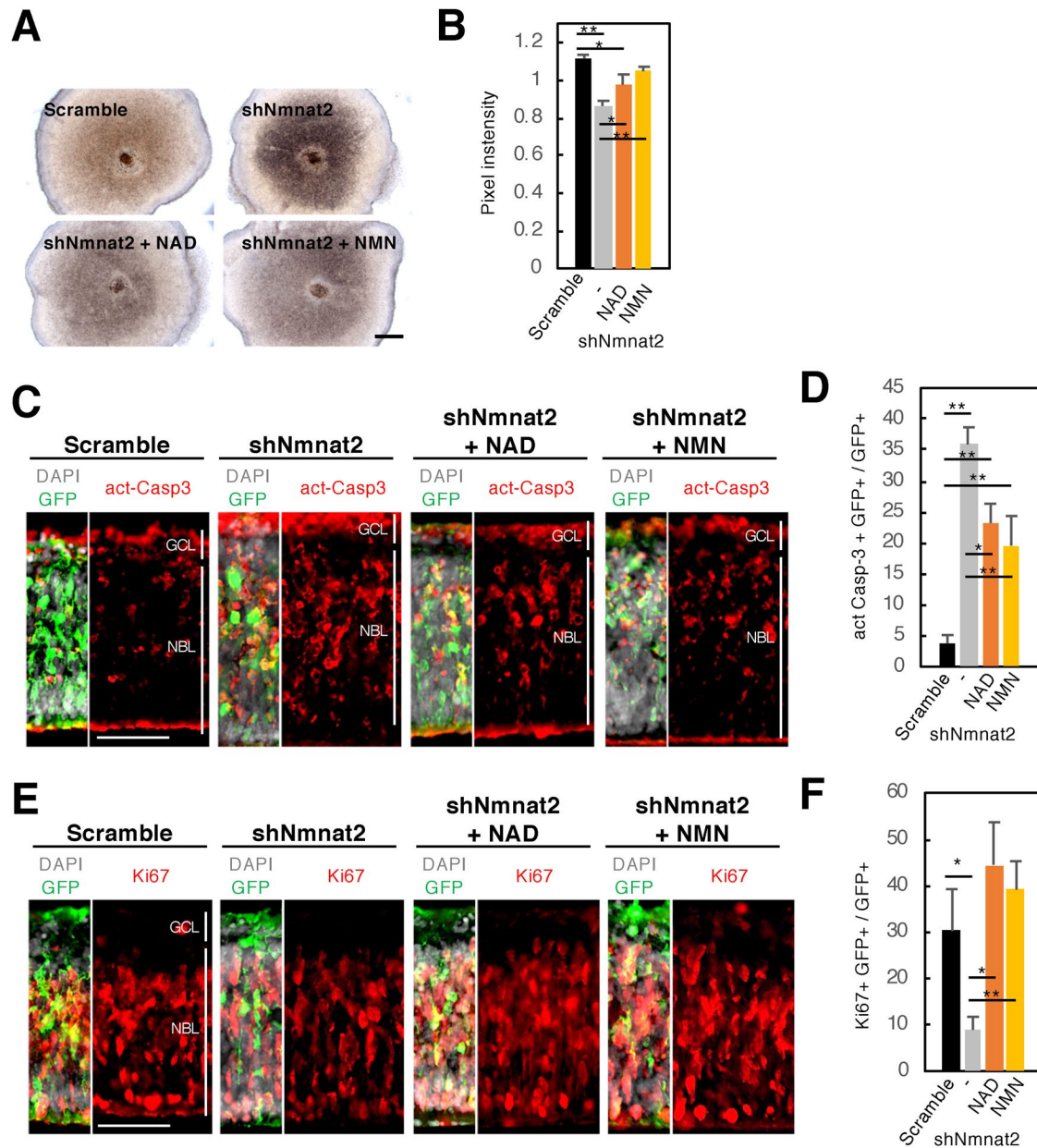


**FIGURE 5:** Evaluation of apoptosis and cell proliferation in shNmnat2-expressing retinas supplemented with NAD or NMN. Retinas isolated from mouse embryos at E17.5 were transfected with scramble sequences or shNmnat2 encoding plasmids and EGFP expressing plasmids. NAD or NMN was present as final concentration at 500  $\mu$ M in the culture media. (A) Brightfield images of flat-mount explant retinas taken from ONL side at day 3 are shown. (B) Black dots, which represent cell death, in panel A were quantified using pixel intensity. Quantified values of the retinas expressing scramble or shNmnat2 with or without NAD or NMN supplementation are shown. (C–F) After 3 d of culture, the explant retinas were harvested. Frozen sections were immunostained with anti-act-Casp3-, C, or anti-Ki67-, E, antibodies. Proportions (%) of act-Casp3+ EGFP+ cells, D, and Ki67+ EGFP+ cells, F, in total EGFP+ cells are shown. Scale bar = 500  $\mu$ m, A, and 50  $\mu$ m, C, and E.

participate in the observed phenotype. To examine the roles of NAD, we cultured explants expressing shNmnat2 or scramble control plasmids in the presence or absence of NAD or NMN. Bright field microscopy showed black dots in the center of the cultured retina, corresponding to dead cells, in the shNmnat2 samples (Figure 5, A and B). Quantitated pixel intensity of the black dots showed their attenuation by administration of NAD or NMN (Figure 5, A and B). Immunohistochemical analysis confirmed that the number of act-Casp3-positive apoptotic cells induced by shNmnat2 expression was decreased by exogenous

NMN or NAD (Figure 5, B and D). Similarly, the decrease in the number of Ki67-positive cells by shNmnat2 was also recovered by NAD or NMN (Figure 5, C and E).

#### Bulk RNA-Seq showed differentially expressed genes in the retinas transfected with shNmnat2 expressing plasmids

We then examined comprehensive transcriptional changes downstream of Nmnat2. As the phenotype associated with the expression of shNmnat2 was completely different from that with expression of shNmnat1 in the previous work (Kuribayashi *et al.*, 2018), we

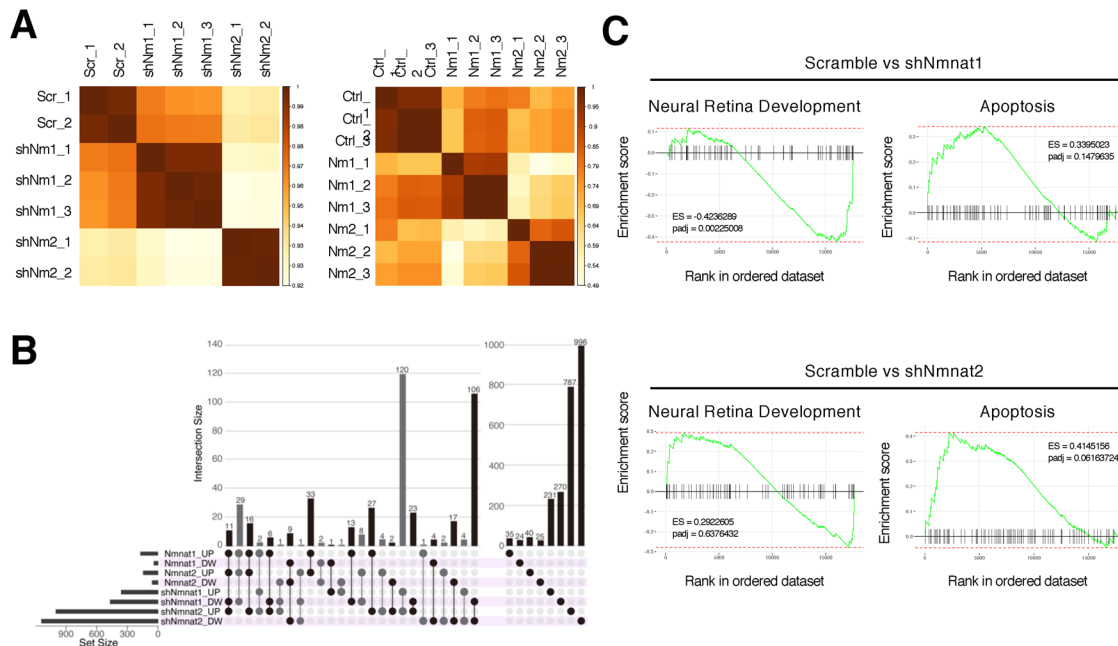


**FIGURE 6:** Similarities and differences between genes regulated by Nmnat1 and Nmnat2. The retinas at P0.5 were cotransfected with pU6-shNmnat1, -shNmnat2, -scramble, pCAG-Nmnat1, -Nmnat2, or pCAG empty vector with pCAG-EGFP and cultured for 3 d. EGFP+ positive cells were purified and used for RNA-Seq. (A) Pearson's correlation coefficient of comprehensive gene expression among scramble (Scr)-, shNmnat1 (shNm1)-, and shNmnat2 (shNm2)-expressing retinas or among control (Ctrl) and Nmnat1 (Nm1)- and Nmnat2 (Nm2)-expressing retinas. Correlation coefficients were calculated using TPM values. (B) Upset plot shows common DEGs among shNmnat1-, shNmnat2-, Nmnat1-, and Nmnat2-expressing retinas. UP indicates up-regulated genes compared with the control, and DW indicates down-regulated genes. (C) GSEA plots were used to evaluate the enrichment of gene sets for neural retina development and apoptosis in shNmnat1- and shNmnat2-expressing retinas.

performed RNA-Seq analysis of shNmnat1- or shNmnat2-expressing retinas. At the same time, we also prepared samples overexpressing Nmnat1 or Nmnat2. The retinas isolated from mice at P0.5 were cotransfected with pU6-shNmnat1 (Kuribayashi *et al.*, 2018), -shNmnat2, -scramble, pCAG-Nmnat1, pCAG-Nmnat2, or pCAG empty vectors (control for overexpression) with pCAG-EGFP, and after 3 d of culture, EGFP-positive cells were purified by cell sorting and used for RNA-Seq analysis. As described in *Materials and Methods*, two samples for scramble- and shNmnat2-, three samples for shNmnat1-, Nmnat1-, Nmnat2-, and control CAG-expressing retinas were used for further detailed analyses (Figure 6A). We compared up-regulated (UP) and down-regulated (DW) genes, and the total number of genes in each category and the number of common genes in multiple samples are shown (Figure 6B). Large numbers of genes were found in shNmnat1-UP vs. shNmnat2-UP and shNmnat1-DW and shNmnat2-DW (Figure 6B). Similarly, more than 30 genes were commonly up-regulated in the Nmnat1- and Nmnat2-expressing retinas (Figure 6B). GSEA analysis showed a significant decrease in expression of the neural retina development gene set in shNmnat1-expressing retinas, while shNmnat2 did not affect expression of these genes (Figure 6C). Enrichment of the apoptotic gene set was not significantly different in comparisons between scramble versus shNmnat1- or shNmnat2-expressing retinas (Figure 6C), suggesting that specific apoptosis-related gene(s) may play pivotal roles in sustaining survival of the retina by Nmnat1 or Nmnat2.

## DISCUSSION

We performed loss-of-function analysis of Nmnat2 in the mouse retina at early, middle, and late developmental stages, and found that Nmnat2 is essential for the survival of retinal cells in the early

and middle periods of development. However, retinal cell differentiation, but not survival, was perturbed at the late developmental stage. Our data indicate that the roles of Nmnat2 change during retinal development. In addition, the effects of shNmnat2 were different from those observed previously with the expression of shNmnat1 (Kuribayashi *et al.*, 2018), strongly suggesting that Nmnat1 and Nmnat2 play distinct roles in retinal development. shNmnat1 and shNmnat2 led to apoptosis in different subpopulations of cells in the retina. In addition, we found no alterations in the expression of *Fas* and *Noxa* by shNmnat2 expression (unpublished data), both of which were strongly induced by shNmnat1 in the retina (Kuribayashi *et al.*, 2018), suggesting that the mechanisms of maintaining retinal cell survival by Nmnat1 and Nmnat2 were different.

We reported previously that global expression levels of *Nmnat1* and *Nmnat2* differed during retinal development (Kuribayashi *et al.*, 2018), and that analysis of public scRNA-Seq data (Clark *et al.*, 2019) provided more details regarding their differential expression patterns in retinal cell subtypes. Therefore, the differences in phenotypes associated with shNmnat1 and shNmnat2 expression may be at least partly explained by the different expression patterns of the two enzymes. Although the expression of *Nmnat2* is low in rod photoreceptors and bipolar cells, we observed decreased numbers of these cell types in shNmnat2-expressing retina. Take our observation of strong apoptosis and reduced proliferation of RPC into consideration, we surmise that the commitment of RPC to the photoreceptor and bipolar cells may be hampered. As another possibility, we cannot exclude that there is no specificity of the effects of Nmnat2 depletion to a certain retinal cell lineage, since photoreceptor and bipolar cells are late-born subtypes, and it is possible

that these cell types are more susceptible to the *Nmnat2* depletion under this experimental condition. As an alternative explanation, low expression level can be more susceptible to *Nmnat2* silencing.

It is also possible that different cell types have different NAD requirements, which may represent the complexity of the effects of NAD synthesis and consumption on cellular homeostasis. In the mature retina, *Nmnat2* was found to have stronger expression in horizontal cells, amacrine cells, and RGCs, but we observed no changes in the distribution or number of BRN3B-positive RGCs by sh*Nmnat2* expression. The reason that might explain this is that most of RGCs had been differentiated at the stages we used for electroporation, and therefore the transfection efficiency of sh*Nmnat2* to the RGCs was very low. The number of TFAP2A-positive amacrine cells was increased, but these amacrine cells were mostly GFP-negative, suggesting that differentiation of RPCs transfected with sh*Nmnat2* expression plasmids into amacrine cells might be prevented by cell death, and that noncell autonomous effects of *Nmnat2* may participate in this phenomenon. Although the expression level of *Nmnat2* in Müller glia was very low, its differentiation was severely perturbed by sh*Nmnat2*, also suggesting possibilities of noncell autonomous effects of sh*Nmnat2* or even that a low level of NMNAT2 plays pivotal roles in Müller glial differentiation. The expression level of *Nmnat1* was relatively high in Müller glia, suggesting that excess NMNAT1 activity affected the development of Müller glia. Furthermore, we observed perturbed localization of CHX10 positive bipolar cells, and it is plausible that structural abnormalities in Müller glia may hamper proper cellular localization of bipolar cells.

Previous reports describing adipogenesis showed that, during adipogenesis, nuclear NAD levels drop concomitantly with rapid induction of NMNAT2, and increased NMNAT2 limits the availability of nuclear NMN, leading to reduced NMNAT1 enzyme activity (Ryu *et al.*, 2018; Majeed *et al.*, 2021). Similarly, it is possible that a reduced NMNAT2 level leads to increased NMNAT1 enzyme activity by inflow of excess NMN from the cytoplasm to the nucleus.

To examine this issue, we performed a comprehensive analysis of the expression patterns of genes that were overexpressed in the retina expressing full-length *Nmnat1* or *Nmnat2* in addition to sh*Nmnat1* or sh*Nmnat2*. These analyses showed that large numbers of genes were commonly up- or down-regulated in the presence of sh*Nmnat1* or sh*Nmnat2*, refuting the possibility of reciprocal NMNAT1 and NMNAT2 enzyme activities by the balance of their expression levels.

Neither *Nmnat1* nor *Nmnat3* can compensate for the loss of *Nmnat2* in *Blad* mutant mice (Hicks *et al.*, 2012), directly indicating their unique roles. Specific roles for *Nmnat2* and *Nmnat1* in the central nervous system have been well documented in diseases, with roles for NMNAT2 in axonal nerve damage (Coleman and Freeman, 2010) and *Nmnat1* in photoreceptor maintenance (Falk *et al.*, 2012; Koenekoop *et al.*, 2012). The roles of their different subcellular localizations (Berger *et al.*, 2005; Lau *et al.*, 2009) in biological functions were not clearly demonstrated, partly because the transport of NAD and related molecules among subcellular compartments remained poorly understood. *Nmnat3* was reported to be localized in mitochondria (Berger *et al.*, 2005), but *Nmnat3* transcript expression level in the retina was extremely low (Kuribayashi *et al.*, 2018). Identification of SLC25A51 as a mammalian mitochondrial NAD transporter (Davila *et al.*, 2018; Luongo *et al.*, 2020) suggested compensatory supply of NAD from the cytoplasm to the mitochondria. Furthermore, mice lacking *Nmnat3* survived and exhibited no overt changes in mitochondrial NAD level (Hikosaka *et al.*, 2014). Therefore, SLC25A51 provided important insights explaining the sharing of the NAD pool, at least between the cytoplasm and mitochondria.

A nuclear NAD transporter has not been identified, but our results strongly suggest that the NAD pool was also shared with the nucleus, as we found that exogenous NMN, which is converted to NAD by NMNAT1, rescued cells from the apoptosis induced by sh*Nmnat2*.

In contrast to the result showing the expression of large number of genes were positively or negatively regulated by *Nmnat2*, both intracellular NAD level and posttranslational modification were not changed in the retina expressing sh*Nmnat2* compared with the control. *Nmnat1*, *Nmnat2*, and *Nmnat3* were reported to show differences in subcellular localization (Berger *et al.*, 2005), but whether these enzymes regulated NAD levels in such segregated territories of cells was unclear, as transporters of NAD and its metabolites among subcellular components were not well documented (Cambonne *et al.*, 2016). Connexin 43 was reported to be a NAD transporter in the plasma membrane (Bruzzone *et al.*, 2001a,b). In fact, we observed that addition of exogenous NAD rescued the retinal phenotype induced by expression of shRNA specific for *Nmnat1* (sh*Nmnat1*), suggesting that NAD can be transported into the intracellular space and probably enters the nucleus (Kuribayashi *et al.*, 2018). In addition, we observed that exogenous NAD also rescued sh*Nmnat2* induced cell apoptosis in this work. As it is unclear whether the level of NAD in subcellular compartments is sufficient to avoid the sharing or scrambling of NAD among NAD users in different compartments, it is possible that balance of *Nmnat* family member expression levels perturb the intracellular dynamics of NAD levels (Ryu *et al.*, 2018) without showing perturbation of global NAD level of whole cell level. Similarly, no global changes in histone acetylation levels were observed, but the possibility remains that changes in specific regions may have occurred. Furthermore, *Nmnat2* is reported to act not only as an NAD synthase but also as a molecular chaperone involving neuronal protection via regulation of protein folding and aggregation. It is possible that *Nmnat2* suppression may have an effect on downstream gene expression through its function as a molecular chaperone.

## MATERIALS AND METHODS

[Request a protocol](#) through *Bio-protocol*.

### Animals

All animal experiments were approved by the Animal Care Committee of the Institute of Medical Science, and Graduate School of Medicine, the University of Tokyo, and conducted in accordance with the ARVO (Association for Research in Vision and Ophthalmology) statement on the use of animals in ophthalmic and vision research. Institute of Cancer Research (ICR) mice were obtained from Japan SLC. Embryonic day (E) 0.5 was defined as the date a vaginal plug was observed for all embryonic mouse tissues analyzed. Eight-week-old mice were defined as "adult mice."

### Construction of shRNA and full length *Nmnats* expressing plasmids

For the construction of shRNA expressing plasmids, the target sequences were determined by siDirect (<http://sidirect2.rnai.jp>). Target sequences were as shown below: Scramble: 5'-aaggtatc-gcaattaatggacgc-3', sh*Nmnat2\_1st*: 5'-aagttctagtctccagttcagg-3', sh*Nmnat2\_2nd*: 5'-aagactaagtctctgataatctat-3'. shRNA expressing plasmids were constructed as described previously (Satoh *et al.*, 2009). Scramble sequences were used for control plasmids (pU6-Scramble). shRNA-expressing plasmids were prepared using

at least two different target sequences (pU6-shNmnat2\_1st and pU6-shNmnat2\_2nd) and we observed essentially the same results between first and second shRNA-expressing plasmids. Target sequences and construction of shRNA expressing plasmids targeting Nmnat1 were shown in our previous study (Kuribayashi *et al.*, 2018). Representative data using shRNA first are shown in the figures. For the construction of overexpressing plasmids of Nmnat1 and Nmnat2, full-length Nmnat1 and Nmnat2 cDNA were synthesized from total RNA purified from mouse retinas by RT-qPCR. The PCR products were subcloned into pGEM-T Easy vector (Promega, USA). Then Nmnat1 and Nmnat2 were inserted into pCAG-KS by using XhoI and NotI sites.

### RNA extraction, cDNA synthesis, and quantitative polymerase chain reaction

Total RNA was purified from mouse retinas using Sepasol RNA I Super G (Nacalai Tesque, Japan), and cDNA was synthesized using ReverTra Ace qPCR RT Master Mix (Toyobo, Japan). A quantitative polymerase chain reaction (qPCR) was performed by the SYBR Green-based method with the Roche Light Cycler 96 (Roche Diagnostics, Japan). *Gapdh* was used as an internal control, and primer sequences were as previously reported (Kuribayashi *et al.*, 2018). To examine the knockdown efficiency of shRNA-expressing plasmids, a total of 100 µg of plasmids containing 80 µg of pU6-shNmnat2 or pU6-Scramble and 20 µg of enhanced green fluorescent protein (EGFP)-expressing plasmids (pCAG-EGFP) were electroporated into NIH3T3 cells with electroporator CUY-21 (Nepa Gene, Japan). After 1–2 d, NIH3T3 cells were treated with trypsin and filtered, and EGFP-positive cells were collected by a cell sorter, FACS Aria SORP (BD Biosciences, USA). Total RNA was purified from the sorted cells, and cDNA was synthesized. Knockdown efficiency of shNmnat2 was examined by qPCR using primer for Nmnat2. Effects of shNmnat2 for the expression of Nmnat1 and Nmnat3 were also examined by RT-qPCR using primers for Nmnat1 or Nmnat3.

### Electroporation and retinal explant culture and measurement of NAD level

In vitro electroporation and retinal explant culture were performed as described previously (Tabata *et al.*, 2004; Iida *et al.*, 2011). A total of 100 µg of plasmids consisting 80 µg of pU6-shNmnat2 or -Scramble and 20 µg of pCAG-EGFP was used for the electroporation. NAD (Tokyo Chemical Industry, Japan) or NMN (Tokyo Chemical Industry, Japan) was added into the culture media at 500 µM (final concentration) for the rescue experiment. NAD content in mice explant retinas was measured using Amplitude™ Fluorimetric NAD/NADH Ratio Assay Kit (AAT Bioquest, USA) according to the manufacturer's instructions. The values of NAD content were divided by the area of explant retinas for normalization.

### Immunohistochemistry

Immunohistochemistry of frozen sections was done as described previously (Tabata *et al.*, 2004; Iida *et al.*, 2011). Primary antibodies used were mouse monoclonal antibodies against Ki67 (BD Bioscience, USA), NR2E3 (photoreceptor-specific nuclear receptor; PNR, PPMX, USA), TFAP2A (DSHB, USA), glutamine synthetase (GS) (Merck, Germany), rabbit polyclonal antibodies against active Caspase 3 (Promega, USA), sheep polyclonal antibody against CHX10 (Exalha Biologicals, USA), calbindin D-28K (Merck, Germany), goat polyclonal antibody against BRN3B (Santa Cruz, USA) and chick polyclonal antibody against GFP (Clontech, USA). Secondary antibodies used were Alexa Fluor 488 or Alexa Fluor 594 conjugated

appropriate secondary antibodies (Life Technologies, USA). Photos were taken under observation using a Zeiss Axio Imager M1 and Axio Imager M2 (Carl Zeiss, Germany).

### Western blot

Western blot was performed as described previously (Kuribayashi *et al.*, 2018). Briefly, mouse retinas were electroporated, and after 3 d of culture, total proteins were extracted. Total proteins (10 µg) in each sample were used for Western blot. Primary antibodies used were mouse monoclonal antibodies against poly ADP ribose (Merck, Germany), acetylated lysine (Merck, Germany), acetylated histone h3 (Merck, Germany), acetylated histone h4 (Merck, Germany) and actin (Merck, Germany), and horseradish peroxidase-linked secondary antibodies (GE Healthcare, USA) were used as secondary antibodies. The chemiluminescent signals were detected with an Amersham Imager 600 (Fuji Film and Cytiva, Japan).

### Bulk RNA-Seq of explant retinas transfected with scramble- or shNmnat2-encoding plasmids

Retinas isolated from mice at P0.5 were transfected with either pU6-Scramble, pU6-shNmnat1, pU6-shNmnat2, control CAG vectors (pCAG empty vectors), pCAG-Nmnat1, or pCAG-Nmnat2 together with pCAG-EGFP. After the retinas were cultured for 3 d as explants, EGFP-expressing cells were collected by a FACS Aria SORP cell sorter (BD Biosciences, USA) as described by Shinoe *et al.* (2010). Total RNAs were extracted from the cells using Sepasol RNA I Super G (Nacalai Tesque, Japan) and quantified by an Agilent 2100 Bioanalyzer (Agilent Technologies, USA). cDNA was synthesized using 1 ng of total RNA and amplified by PCR by a SMART-Seq v4 Ultra Low Input RNA Kit for Sequencing (Takara, Japan) according to the manufacturer's instructions. The RNA-Seq libraries were prepared using the amplified cDNA and Nextera XT DNA Sample Preparation Kit (Illumina, USA). Single-read sequencing (36 bp) was conducted by a HiSeq3000 sequencer (Illumina, USA).

### Analysis of bulk RNA-Seq dataset

Sequenced reads were mapped to the mouse transcriptome (GENCODE GRCm38.p6) with salmon v0.11.3.27. Salmon output was converted using wasabi v0.327 and loaded into sleuth v0.30.028 for further downstream analysis, including calculation of transcripts per million (TPM). We prepared three independent samples for each condition, and using Pearson's correlation coefficient as an indicator, samples with large errors among the samples with the same condition were excluded, and finally two samples for the scramble- and shNmnat2-, three samples for shNmnat1-, Nmnat1-, Nmnat2-, and control CAG-expressing retinas were used for further detailed analyses. Salmon output was also converted using tximeta v1.8.5 and loaded into DESeq2 v1.30.1 for identification of differentially expressed genes (DEGs). Gene set enrichment analysis (GSEA) was performed to generate enrichment plots for selected gene sets using the R package fgsea. DESeq2 output was processed on neural retina development gene set and apoptosis gene set using the R package fgsea. Gene ontology (GO) term enrichment analysis was performed using the Database for Annotations, Visualization and Integrated Discovery (DAVID). Data visualization was performed using R packages, ggplot2, EnhancedVolcano and UpSetR.

### Re-analysis of publicized single cell RNA-Seq data

Reanalysis of the single-cell RNA-Seq (scRNA-Seq) dataset from GSE118614 was performed by the R package Seurat v4.0.4 (Stuart *et al.*, 2019; Hao *et al.*, 2021). Count matrix, cellular phenotype

data, and feature data downloaded at [https://github.com/gofflab/developing\\_mouse\\_retina\\_scRNASeq](https://github.com/gofflab/developing_mouse_retina_scRNASeq) were loaded into Seurat to generate a gene count matrix (Clark *et al.*, 2019). Nonretinal cell types were removed based on the cellular phenotype data, and then damaged cells and doublet cells were also removed by quality control of Seurat. Cells showing >600 genes, >2000 count of RNA reads, and <10% expression of mitochondrial genes were used for downstream analysis. We visualized cell clusters using the uniform manifold approximation and projection (UMAP) dimensionality reduction.

### Quantitative analysis of dead cell regions in retinal explants

Brightfield images of flat-mount explant retinas transfected with scramble- or shNmnat2-expressing plasmids at E17.5 were taken at day 3. Retinal regions transfected with the plasmids were defined by EGFP fluorescence, and the average of pixel intensity of the transfected region of the retinas was quantified by ImageJ v1.53i to estimate the impact of shNmnat2 and the administration of NAD or NMN on the cell death. The values are means and standard deviations calculated by using three independent samples.

### Statistical analysis

All graphs are means with SD that were calculated from at least three independent samples. The *p*-values were calculated by two-tailed Student's *t* test (Figure 2, G–I, Figures 3 and 4) or one-way ANOVA followed by Tukey's multiple comparison test (Figure 2, B and C, and Figure 5); \**p* < 0.05, \*\**p* < 0.01.

### Data availability

The GEO accession number of the RNA-Seq dataset generated for this study is GSE197192. The GEO accession numbers of public datasets used for secondary analysis of bulk RNA-Seq are GSE71462 (Ueno *et al.*, 2016) and GSE87064 (Aldiri *et al.*, 2017), and that of scRNA-Seq is GSE118614 (Clark *et al.*, 2019).

### ACKNOWLEDGMENTS

This work was supported by JSPS KAKENHI Grants 16H06279(PAGS), 18K16919, and 20K18376. The authors thank Masaya Fukushima and Akira Murakami (Juntendo University) for fruitful discussion.

### REFERENCES

Aldiri I, Xu B, Wang L, Chen X, Hiler D, Griffiths L, Valentine M, Shirinifard A, Thiagarajan S, Sablauer A, *et al.* (2017). The dynamic epigenetic landscape of the retina during development, reprogramming, and tumorigenesis. *Neuron* 94, 550–568.e10.

Ali YO, Li-Kroeger D, Bellen HJ, Zhai RG, Lu HC (2013). NMNATs, evolutionarily conserved neuronal maintenance factors. *Trends Neurosci* 36, 632–640.

Berger F, Lau C, Dahlmann M, Ziegler M (2005). Subcellular compartmentation and differential catalytic properties of the three human nicotinamide mononucleotide adenylyltransferase isoforms. *J Biol Chem* 280, 36334–36341.

Bruzzone S, Franco L, Guida L, Zocchi E, Contini P, Bisso A, Usai C, De Flora A (2001a). A self-restricted CD38–connexin 43 cross-talk affects NAD<sup>+</sup> and cyclic ADP-ribose metabolism and regulates intracellular calcium in 3T3 fibroblasts. *J Biol Chem* 276, 48300–48308.

Bruzzone S, Guida L, Zocchi E, Franco L, De Flora A (2001b). Connexin 43 hemi channels mediate Ca<sup>2+</sup>-regulated transmembrane NAD<sup>+</sup> fluxes in intact cells. *FASEB J* 15, 10–12.

Cambronne XA, Stewart ML, Kim DH, Jones-Brunette MA, Morgan RK, Farrens DL, Cohen MS, Goodman RH (2016). Biosensor reveals multiple sources for mitochondrial NAD<sup>+</sup>. *Science* (80-) 352, 1474–1477.

Cepko CL, Austin CP, Yang X, Alexiades M, Ezzedine D (1996). Cell fate determination in the retina. *Proc Natl Acad Sci USA* 93, 589–595.

Clark BS, Stein-O'Brien GL, Shiao F, Cannon GH, Davis-Marcisak E, Sherman T, Santiago CP, Hoang TV, Rajaii F, James-Esposito RE, *et al.* (2019).

Single-cell RNA-seq analysis of retinal development identifies NFI factors as regulating mitotic exit and late-born cell specification. *Neuron* 102, 1111–1126.e5.

Coleman MP, Freeman MR (2010). Wallerian degeneration, WldS, and Nmnat. *Annu Rev Neurosci* 33, 245–267.

Conforti L, Gilley J, Coleman MP (2014). Wallerian degeneration: an emerging axon death pathway linking injury and disease. *Nat Rev Neurosci* 15, 394–409.

Covarrubias AJ, Perrone R, Grozio A, Verdin E (2021). NAD<sup>+</sup> metabolism and its roles in cellular processes during ageing. *Nat Rev Mol Cell Biol* 22, 119–141.

Davila A, Liu L, Chellappa K, Redpath P, Nakamaru-Ogiso E, Paoletta LM, Zhang Z, Migaud ME, Rabinowitz JD, Baur JA (2018). Nicotinamide adenine dinucleotide is transported into mammalian mitochondria. *Elife* 7, e33246.

den Hollander AI, Roepman R, Koenekoop RK, Cremers FPM (2008). Leber congenital amaurosis: genes, proteins and disease mechanisms. *Prog Retin Eye Res* 27, 391–419.

Essuman K, Summers DW, Sasaki Y, Mao X, DiAntonio A, Millbrandt J (2017). The SARM1 toll/interleukin-1 receptor domain possesses intrinsic NAD<sup>+</sup> cleavage activity that promotes pathological axonal degeneration. *Neuron* 93, 1334–1343.

Falk MJ, Zhang Q, Nakamaru-Ogiso E, Kannabiran C, Fonseca-Kelly Z, Chakarova C, Audo I, MacKay DS, Zeitz C, Borman AD, *et al.* (2012). NMNAT1 mutations cause Leber congenital amaurosis. *Nat Genet* 44, 1040–1045.

Feng Y, Yan T, Zheng J, Ge X, Mu Y, Zhang Y, Wu D, Du JL, Zhai Q (2010). Overexpression of WldS or Nmnat2 in mauthner cells by single-cell electroporation delays axon degeneration in live zebrafish. *J Neurosci Res* 88, 3319–3327.

Finnin MS, Donigian JR, Pavletich NP (2001). Structure of the histone deacetylase SIRT2. *Nat Struct Biol* 8, 621–625.

Gilley J, Coleman MP (2010). Endogenous Nmnat2 is an essential survival factor for maintenance of healthy axons. *PLoS Biol* 8, e1000300.

Gilley J, Orsomando G, Nascimento-Ferreira I, Coleman MP (2015). Absence of SARM1 rescues development and survival of NMNAT2-deficient axons. *Cell Rep* 10, 1975–1982.

Greenwald SH, Charette JR, Staniszewska M, Ying Shi L, Brown SD, Stone L, Liu Q, Hicks WL, Collin GB, Bowl MR, *et al.* (2016). Mouse models of NMNAT1–Leber congenital amaurosis (LCA9) recapitulate key features of the human disease. *Am J Pathol* 186, 1925–1938.

Hao Y, Hao S, Andersen-Nissen E, Mauck WM, Zheng S, Butler A, Lee MJ, Wilk AJ, Darby C, Zager M, *et al.* (2021). Integrated analysis of multi-modal single-cell data. *Cell* 184, 3573–3587.

Hicks AN, Lorenzetti D, Gilley J, Lu B, Andersson KE, Miligan C, Overbeek PA, Oppenheim R, Bishop CE (2012). Nicotinamide mononucleotide adenylyltransferase 2 (Nmnat2) regulates axon integrity in the mouse embryo. *PLoS One* 7, 1–10.

Hikosaka K, Ikutani M, Shito M, Kazuma K, Gulshan M, Nagai Y, Takatsu K, Konno K, Tobe K, Kanno H, *et al.* (2014). Deficiency of nicotinamide mononucleotide adenylyltransferase 3 (nmnat3) causes hemolytic anemia by altering the glycolytic flow in mature erythrocytes. *J Biol Chem* 289, 14796–14811.

Iida A, Shinoue T, Baba Y, Mano H, Watanabe S (2011). Dicer plays essential roles for retinal development by regulation of survival and differentiation. *Investig Ophthalmol Vis Sci* 52, 3008–3017.

Imai S, Guarente L (2016). It takes two to tango: NAD<sup>+</sup> and sirtuins in aging/longevity control. *npj Aging Mech Dis* 2, 16017.

Kim MY, Mauro S, Gérvy N, Lis JT, Kraus WL (2004). NAD<sup>+</sup>-dependent modulation of chromatin structure and transcription by nucleosome binding properties of PARP-1. *Cell* 119, 803–814.

Koenekoop RK, Wang H, Majewski J, Wang X, Lopez I, Ren H, Chen Y, Li Y, Fishman GA, Genead M, *et al.* (2012). Mutations in NMNAT1 cause Leber congenital amaurosis and identify a new disease pathway for retinal degeneration. *Nat Genet* 44, 1035–1039.

Kuribayashi H, Baba Y, Iwagawa T, Arai E, Murakami A, Watanabe S (2018). Roles of Nmnat1 in the survival of retinal progenitors through the regulation of pro-apoptotic gene expression via histone acetylation. *Cell Death Dis* 9, 891.

Lau C, Niere M, Ziegler M (2009). The NMN/NaMN adenylyltransferase (NMNAT) protein family. *Front Biosci* 14, 410–431.

Luongo TS, Eller JM, Lu M-J, Niere M, Raith F, Perry C, Bornstein MR, Oliphant P, Wang L, McReynolds MR, *et al.* (2020). SLC25A51 is a mammalian mitochondrial NAD(+) transporter. *Nature* 588, 174–179.

Mack TG, Reiner M, Beirowski B, Mi W, Emanuelli M, Wagner D, Thomson D, Gillingwater T, Court F, Conforti L, *et al.* (2001). Wallerian degeneration

- of injured axons and synapses is delayed by a Ube4b/Nmnat chimeric gene. *Nat Neurosci* 4, 1199–1206.
- Majeed Y, Halabi N, Madani AY, Engelke R, Bhagwat AM, Abdeselem H, Agha MV, Vakayil M, Courjaret R, Goswami N, et al. (2021). SIRT1 promotes lipid metabolism and mitochondrial biogenesis in adipocytes and coordinates adipogenesis by targeting key enzymatic pathways. *Sci Rep* 11, 8177.
- Ruan K, Zhu Y, Li C, Brazill JM, Zhai RG (2015). Alternative splicing of *Drosophila* Nmnat functions as a switch to enhance neuroprotection under stress. *Nat Commun* 6, 10057.
- Ryu KW, Nandu T, Kim J, Challa S, DeBerardinis RJ, Lee Kraus W (2018). Metabolic regulation of transcription through compartmentalized NAD<sup>+</sup> biosynthesis. *Science* (80-) 360.
- Satoh S, Tang K, Iida A, Inoue M, Kodama T, Tsai SY, Tsai MJ, Furuta Y, Watanabe S (2009). The spatial patterning of mouse cone opsin expression is regulated by bone morphogenetic protein signaling through downstream effector COUP-TF nuclear receptors. *J Neurosci* 29, 12401–12411.
- Shinoe T, Kuribayashi H, Saya H, Seiki M, Aburatani H, Watanabe S (2010). Identification of CD44 as a cell surface marker for Müller glia precursor cells. *J Neurochem* 115.
- Stuart T, Butler A, Hoffman P, Hafemeister C, Papalexi E, Mauck WM, Hao Y, Stoeckius M, Smibert P, Satija R (2019). Comprehensive integration of single-cell data. *Cell* 177, 1888–1902.
- Tabata Y, Ouchi Y, Kamiya H, Manabe T, Arai K, Watanabe S (2004). Specification of the retinal fate of mouse embryonic stem cells by ectopic expression of Rx/rax, a homeobox gene. *Mol Cell Biol* 24, 4513–4521.
- Ueno K, Iwagawa T, Kuribayashi H, Baba Y, Nakauchi H, Murakami A, Nagasaki M, Suzuki Y, Watanabe S (2016). Transition of differential histone H3 methylation in photoreceptors and other retinal cells during retinal differentiation. *Sci Rep* 6, 29264.
- Young RW (1985). Cell differentiation in the retina of the mouse. *Ant Rec* 212, 199–205.
- Zhai RG, Zhang F, Hiesinger PR, Cao Y, Haueter CM, Bellen HJ (2008). NAD synthase NMNAT acts as a chaperone to protect against neurodegeneration. *Nature* 452, 887–91.